Journal of Crystal Growth 352 (2012) 106–109

Contents lists available at SciVerse ScienceDirect

Journal of Crystal Growth

journal homepage: www.elsevier.com/locate/jcrysgro

Crystal growth and dopant segregation of Ce:LiSrAlF$_6$ and Eu:LiSrAlF$_6$ crystals with high dopant concentrations

A. Yamaji [a], Y. Yokota [a], T. Yanagida [b], N. Kawaguchi [c], Y. Futami [b], Y. Fujimoto [a,b,c], A. Yoshikawa [a,b,*]

[a] Institute for Materials Research, Tohoku University, 2-1-1 Katahira, Aoba-ku, Sendai 980-8577, Japan
[b] New Industry Creation Hatchery Center, Tohoku University, 6-6-10 Aoba, Aramaki, Aoba-ku, Sendai 980-8579, Japan
[c] Tokuyama Corporation, Shibuya 3-chome, Shibuya, Tokyo 150-8383, Japan

ARTICLE INFO

Available online 8 February 2012

Keywords:
A1. Doping
A1. Segregation
A2. Growth from melt
B2. Scintillator materials

ABSTRACT

Ce:LiSrAlF$_6$ and Eu:LiSrAlF$_6$ crystals with different dopant concentrations were grown by the micro-pulling-down method. The crystals with high dopant crystal included the secondary phase as clusters with the plate shape in BSE images. The secondary phases were identified CeF_3 and EuF_2, respectively, by the EDS analysis and powder-XRD measurement. Eu concentration against the Sr sites in the Eu 2% doped LiSAF crystal were most uniform in the range 0.9–1.6 atm% using the EPMA.

1. Introduction

Ce doped colquiriite crystals such as LiSrAlF$_6$ (LiSAF) and LiCaAlF$_6$ (LiCAF) crystals [1–3] have been investigated for UV laser materials since 1990 s and proved as good host lattices for optical materials. For the high performance of Ce doped colquiriite crystal, Czochralski (Cz) growth process and optimum condition of Ce^{3+} doping levels in crystals have been developed [4,5]. In recent years, we have a great deal to apply LiSAF and LiCAF crystals for scintillation materials, which have been widely used for medical application, security and so on. We developed Ce or Eu doped colquiriite crystals for thermal neutron detection which showed appropriate properties [6–9], and then are approaching higher performances to optimize the crystal growth process and doping. In the case of LiSAF, three cations are located in octahedral sites with the difference in sizes and charges. Considering the ionic radius of the Ce^{3+} ion (1.17 Å), Ce^{3+} ions are assumed to preferentially substitute into the Sr^{2+} sites rather than Li^+ or Al^{3+} sites. Against the Sr^{2+} ionic radius of 1.30 Å which is larger enough than Ce^{3+} ionic radius, the Li^+ and Al^{3+} ionic radii are 0.88 Å and 0.67 Å, respectively [10]. In the same way, the substitution of Eu^{3+} ion (1.09 Å) is considered to be preferred into $Sr2^+$ sites, where the Eu^{2+} ions (1.31 Å) were found to be located as confirmed by spectroscopy.

In this report, we focused on the crystal growth of Ce:LiSAF and Eu:LiSAF by the micro-pulling-down [11], and these dopant segregations. In our past work, the scintillation properties of LiSAF crystals depended on the dopant concentration [12], however the dependence on the real concentration in the crystal was not demonstrated. Investigation of the dopant segregation would develop the scintillation properties.

2. Experimental procedure

2.1. Crystal growth

The LiF (95% ^{6}Li), SrF_2, AlF_3, CeF_3 and EuF_3 of 4 N purity were used as starting materials to prepare powder mixtures with nominal chemical compositions of Li $(Sr_{1-x}\ Ce_x)\ AlF_6$ (x=0.0025, 0.0050, 0.010, 0.020 and 0.030) and Li $(Sr_{1-y}\ Eu_y)\ AlF_6$ (y=0.0025, 0.010, 0.020, 0.030 and 0.040). The mixtures were placed in a graphite crucible and the crucible was set in the center of the RF coil in the vacuum-tight chamber.

The chamber was evacuated up to 10^{-3} Pa and the crucible was heated up to 600 °C using an RF heating system and kept for 6 h at this temperature to remove oxygen traces caused by the moisture of raw materials and adsorbates on the chamber surface. After the baking process, the chamber reached to $\sim 10^{-4}$ Pa. Then, the chamber was filled with the mixture of 90% Ar (99.9999%) and 10% CF_4 (99.999%) gas until ambient pressure. The crucible was heated up to about 750 °C above the melting temperature of LiSAF. A platinum wire was used as the seed for crystal growth, and the crystal growth rate was 0.1 mm/min. The as-grown crystal had 2–3 mm diameter.

In the case of crystal growth for LiSAF ($x > 1.0$, $y > 2.0$) with high dopant concentrations, the melt was expanded along the bottom of a crucible and the stable crystal growth was difficult.

* Corresponding author at: Institute for Materials Research, Tohoku University, 2-1-1 Katahira, Aoba-ku, Sendai 980-8577, Japan. Tel.: +81 22 217 5167; fax: +81 22 217 5102.
E-mail address: yosikawa@tagen.tohoku.ac.jp (A. Yoshikawa).

0022-0248/$ - see front matter © 2012 Elsevier B.V. All rights reserved.
doi:10.1016/j.jcrysgro.2012.02.001

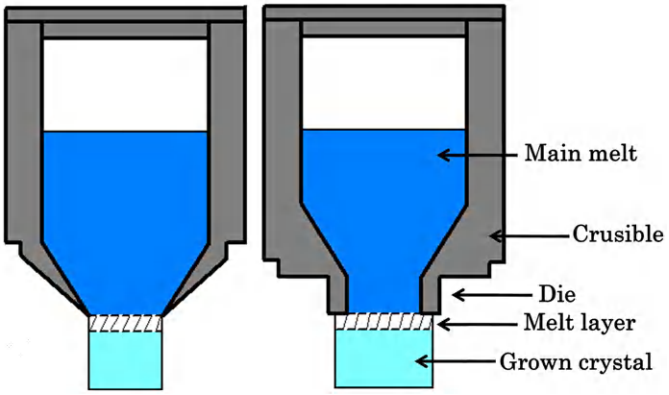

Fig. 1. Schematic diagrams of normal and modified crucible.

Therefore, we used a crucible with a columnar die in 3 mm diameter at the bottom, which has a hole in 2 mm diameter. The schematic diagrams of normal and modified crucible are shown in Fig. 1. The expansion of the melt was limited by the cross-section of the bottom of the die.

2.2. Phase characterization

Parts of the grown crystals were crushed and perfectly ground into fine powders. To identify the phases of grown crystals, powder X-Ray Diffraction (XRD) using RINT-2000 (RIGAKU) was carried out in the 2θ range from 20° to 80°. The X-ray source was CuKα (accelerating voltage: 40 kV, beam current: 40 mA).

To identify the distribution of secondary phase, the character X-rays from samples were detected using Scanning Electron Microscope (SEM) (Hitachi, S-3400N) with Energy Dispersive X-ray Spectroscopy (EDS) (Horiba, EDX, EMAX X-act). The chemical compositions and dopants distribution in the grown crystals were analyzed by the Electron Probe Micro Analysis (EPMA) using INCA Wave (Oxford Instruments) along the growth direction (step=2 mm).

Segregation coefficients of Eu^{2+} and Eu^{3+} can be different because of the Goldschmidt rule. Eu^{2+} and Eu^{3+} ions can coexist in the crystals. For the simple estimation of the ratio of divalent and trivalent Eu ions, the radioluminescence spectra of the portions of the crystal were measured using the Spectrometer FLS920 (Edinburgh Instruments) with 5.5 MeV alpha-ray from a ^{241}Am isotope. The ratio of ions approximates to that of radioluminescence intensityies from Eu^{2+} 5d–4f transition and Eu^{3+} 4f–4f transition.

3. Results and discussion

3.1. Crystal growth

We have succeeded to grow Ce and Eu doped crystals and the grown crystals and the polished crystals which could be observed inside were shown in Fig. 2. While samples with low dopant concentrations were transparent, those with high dopant concentrations had milky parts and were opaque due to the secondary phase inside of the obtained crystal. The crystals grown by modified crucible are 2 mm in diameter. The transparent and milky parts were cleary distinguished in Eu:LiSAF and they concentrated on the central region and the rim in the radial direction, respectively.

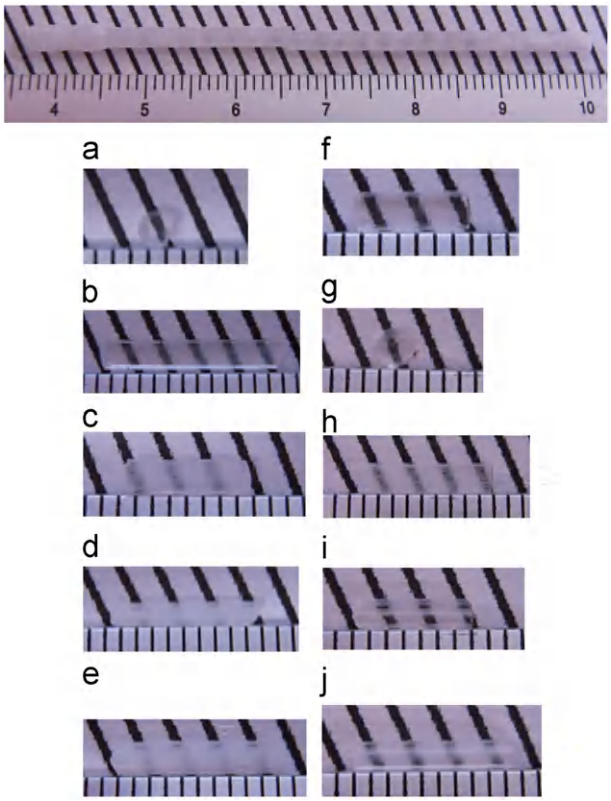

Fig. 2. View of an as-grown Eu 2% doped LiSAF crystal (top) and those of the cross-sections by μ–PD method ((a) $x=0.0025$, (b) $x=0.0050$, (c) $x=0.010$, (d) $x=0.020$, (e) $x=0.030$, (f) $y=0.0025$, (g) $y=0.010$, (h) $y=0.020$, (i) $y=0.030$ and (j) $y=0.040$).

3.2. Phase characterization

The cross-section of perpendicular to the growth direction were observed using SEM, as shown in Fig. 3. The secondary phase with amounts of heavy elements observed as clusters with the plate shape on Back Scattered Electron (BSE) images. For the measurements of chemical composition, both the areas of main phase and the clusters were detected with EDS, in Fig. 4. In the area where clusters were not included, the character X-rays of Ce were hardly observed. On the other hand, Ce was clearly detected in the area where clusters were included. In the previous study, the real doping percentage of Ce^{3+} in the LiSAF grown by Cz method was approximately 0.02 mol% [5] which is difficult to detect with X-ray and so the clusters were composed of rich Ce impurity phase. In the case of Eu:LiSAF, the impurity phase was also distributed similar form and clusters were composed of Eu ions.

In Fig. 5 the LiSAF single phase of the flurite-type structure with space group of P31c was confirmed in samples with high dopants concentrations from the powder XRD. On the other hand, the diffraction peaks of from the phases of CeF_3 and EuF_2 as well as $LiSAF_6$ were observed in those with high dopants concentrations. Based on these chemical composition analyses, each impurity phases were identified as clusters of CeF_3 for Ce:LiSAF and EuF_2 for Eu:LiSAF, respectively.

To evaluate the distribution of Eu and Sr, EPMA measurements were performed on the sample cutting from the Eu 2% doped LiSAF crystal. Unfortunately, the distribution coefficient was not able to be precisely calculated due to the secondary phase of EuF_2, the Eu concentration in the melt would be higher than that in the single phase. In this case, only the transparent phase was measured along the crystal growth axis and the Eu concentration against the solidification was displayed in Fig. 6. The Eu

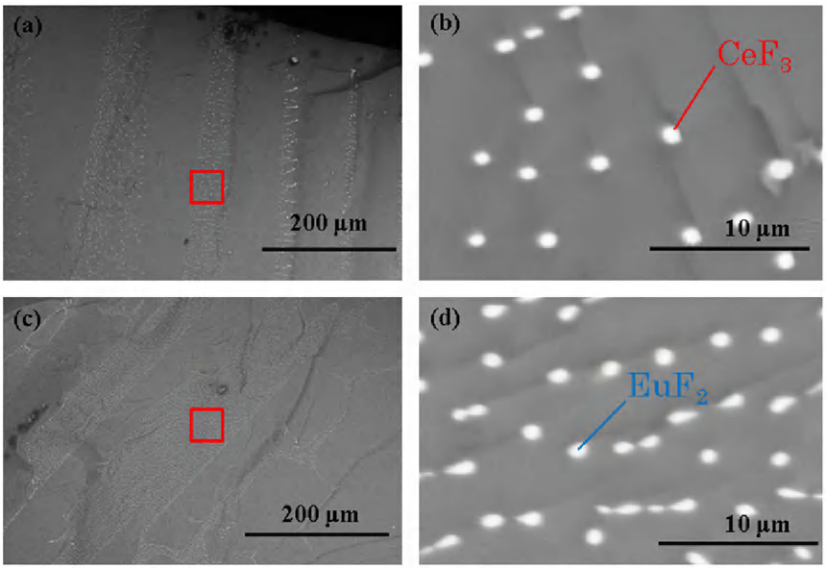

Fig. 3. BSE images of (a), (c) Ce 3% and Eu 4% doped LiSAF in low magnification and (b), (d) which were magnified in the (a), (c) areas closed red lines, respectively (For interpretation of the references to color in this figure legend, the reader is referred to the web version of this article.).

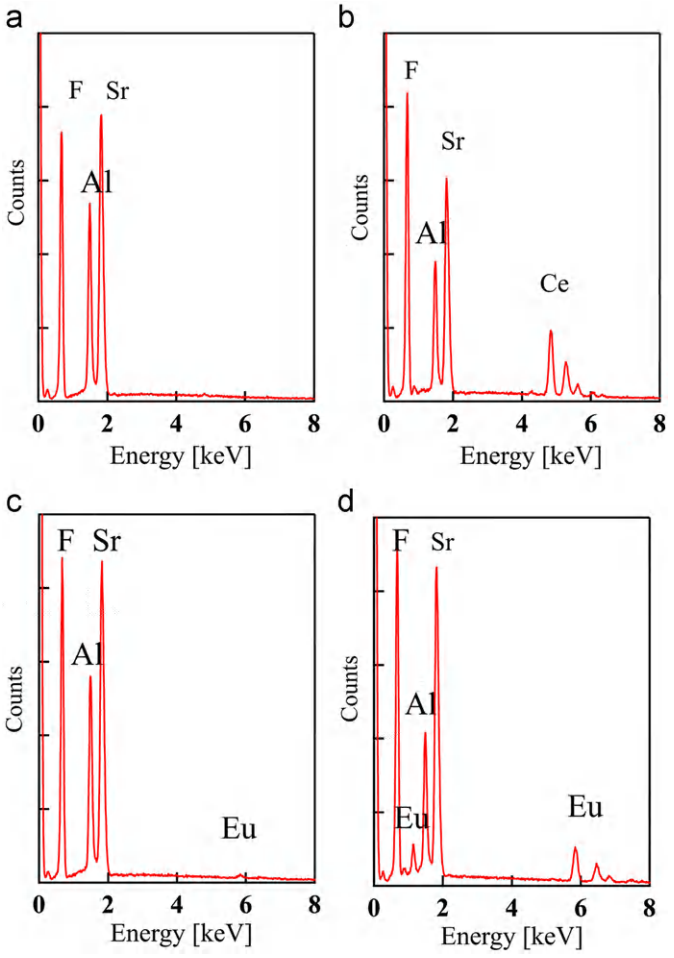

Fig. 4. EDS spectra of: (a) the area where clusters were not included in Ce:LiCAF, (b) the area where clusters were included in Ce:LiCAF, (c) the area where clusters were not included in Eu:LiCAF and (d) the area where clusters were included in Eu:LiCAF.

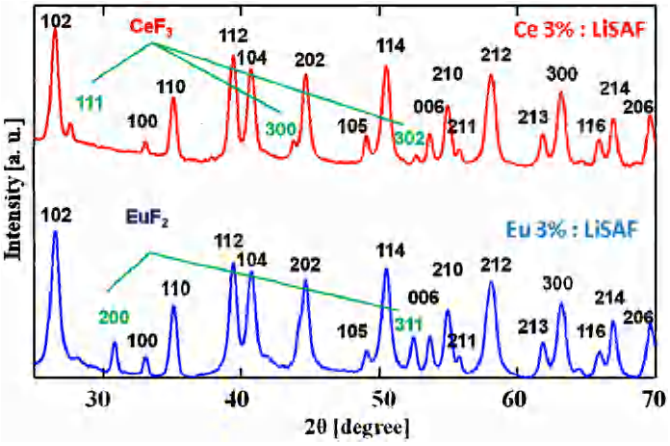

Fig. 5. Powder XRD patterns of Ce 3% (upper) and Eu 4% (lower) doped LiSAF crystals.

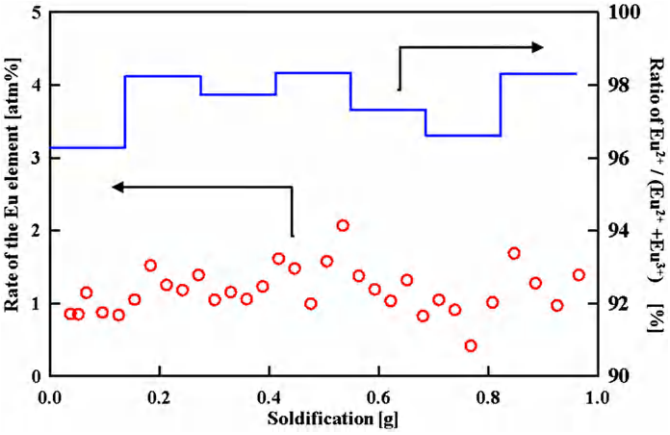

Fig. 6. Eu distribution along growth axis of Eu 2% doped LiSAF (dot) and the ratio of Eu^{2+} to Eu^{3+} ions in the crystal (line).

concentration in Sr sites was distributed most uniformly among the range 0.9–1.6 atm% through the whole crystals. The Ce concentration in the Ce:LiSAF crystal was less than the measurement limitation of EPMA whose signal intensity was equaled to the back ground. The ratio of Eu^{2+} ions in the crystals was constantly hiegher than 96% through the whole crystal

because the radius of Eu^{2+} is closer to that of Sr^{2+} than that of Eu^{3+} and has same valence state as Sr^{2+}.

4. Conclusions

We grew Ce:LiSAF and Eu:LiSAF crystals by the micro-pulling-down method. The grown crystals with high dopant concentration included the secondary phases which were observed as clusters with the plate shape on the BSE image. They were identified CeF_3 and EuF_2, respectively, by the EDS analysis and powder-XRD measurement. Eu concentration was uniform around 0.9 to 1.6 atm% in LiSAF, when it was grwn from the Eu 2 atm% LiSAF melt, however Ce concentration was less than the measurement limitation of EPMA. Further investigation into the segregation of LiSAF crystals needs the precise chemical composition concentration measurement such as the Inductively Coupled Plasma Mass Spectrometry (ICP-MS) analysis and a large sized crystal grown by the Cz method.

References

[1] M.A. Dubinskii, V.V. Semanshko, A.K. Naumov, R.Yu. Abdulsabirov, S.L. Korableva, Journal of Modern Optics 40 (1993) 1–5.
[2] J.F. Pinto, G.H. Rosenblatt, L. Esterowitz, G.J. Quarles, Electronics Letters 30 (1994) 240–241.
[3] C.D. Marshall, J.A. Speth, S.A. Payne, W.P. Krupke, G.J. Quarles, V. Castillo, B.H.T. Chai, Journal of the Optical Society of America B: Optical Physics 11 (1994) 2054–2065.
[4] Kiyoshi Shimamura, Sonia L Baldochi, Izilda M Ranieri, Hiroki Sato, Tomoyo Fujita, Vera L Mazzocchi, Carlos B.R Parente, Carlos O Paiva-Santos, Celso V Santilli, Nobuhiko Sarukura, Tsuguo Fukuda, Journal of Crystal Growth 223 (3) (2001) 383–388.
[5] Vida K. Castillo, Gregory J. Quarles, Journal of Crystal Growth 174 (1–4) (1997) 337–341.
[6] A. Yoshikawa, T. Yanagida, Y. Yokota, N. Kawaguchi, S. Ishizu, K. Fukuda, T. Suyama, K.J. Kim, J. Pejchal, M. Nikl, K. Watanabe, M. Miyake, M. Baba, K. Kamada, IEEE Transactions on Nuclear Science 56 (2009) 3796–3799.
[7] T. Yanagida, A. Yoshikawa, Y. Yokota, S. Maeo, N. Kawaguchi, S. Ishizu, K. Fukuda, T. Suyama, Optical Materials 32 (2) (2009) 311–314.
[8] T. Yanagida, N. Kawaguchi, Y. Fujimoto, K. Fukuda, Y. Yokota, A. Yamazaki, K. Watanabe, J. Pejchal, A. Uritani, T. Iguchi, A. Yoshikawa, Optical Materials 33 (2011) 1243–1247.
[9] Takayuki Yanagida, Noriaki Kawaguchi, Yutaka Fujimoto, Yuui Yokota, Atsushi Yamazaki, Kenichi Watanabe, Kei Kamada, Akira Yoshikawa and Valery Chani, Rad. Meas. In press doi:10.1016/j.radmeas.2011.04.034.
[10] R.D. Shanon, C.T. Prewitt, Acta Crystallography 4 (1969) 925.
[11] A. Yoshikawa, T. Satonaga, K. Kamada, H. Sato, M. Nikl, N. Solovieva, T. Fukuda, Journal of Crystal Growth 270 (2004) 427–432.
[12] Akihiro Yamaji, Takayuki Yanagida, Noriaki Kawaguchi, Yutaka Fujimoto, Yuui Yokota, Kenichi Watanabe, Atsushi Yamazaki, Akira Yoshikawa, Jan Pejchal, Nucl. Instrum. Meth-A, in press.